

Numerical Study of the Roberge-Weiss Transition.

V. G. Bornyakov

*Institute for High Energy Physics NRC “Kurchatov Institute”, 142281 Protvino, Russia
Institute of Theoretical and Experimental Physics NRC “Kurchatov Institute”, 117218 Moscow, Russia*

N. V. Gerasimeniuk, V. A. Goy, A. A. Korneev, and A. V. Molochkov
Pacific Quantum Center, Far Eastern Federal University, 690922 Vladivostok, Russia

A. Nakamura

*RCNP, Osaka University, Osaka 567-0047, Japan and
Pacific Quantum Center, Far Eastern Federal University, 690922 Vladivostok, Russia*

R. N. Rogalyov

*Institute for High Energy Physics NRC “Kurchatov Institute”,
142281 Protvino, Russia*

We study numerically the Roberge-Weiss (RW) phase transition associated with the discontinuities in the quark-number density at definite values of imaginary quark chemical potential. The quark number density ρ is parametrized by the polynomial fit functions and this parametrization is used to compute the canonical partition functions. It is demonstrated that this approach provides a good framework for the analysis of lattice QCD data at finite density and $T > T_{RW}$. We argue that at high temperatures the Lee-Yang zeroes (LYZ) lie on the negative real semiaxis provided that the high-quark-number contributions to the grand canonical partition function are properly taken into account. We find nonzero linear density of the LYZ distribution which signals the RW phase transition.

PACS numbers: 11.15.Ha, 12.38.Gc, 12.38.Aw

Keywords: Quantum chromodynamics, Lee-Yang zeros, Roberge-Weiss transition

I. INTRODUCTION

Properties of strong-interacting matter at nonzero temperature T and quark chemical potential μ_q have received considerable attention. QCD phase diagram in the $T - \mu_q$ plane is expected to have a rich structure, which can be studied experimentally in high-energy nuclear collisions and astronomical observations of the neutron stars. For many years, it had been thought that the lattice-QCD simulations at finite μ_q are impossible because of the sign problem. And yet, thanks to recent developments, now one can access the regions at finite T and μ_q up to $\mu_q/T \sim 2$, see, e.g. [1, 2].

When the chemical potential is pure imaginary, $\mu_q = i\mu_{qI}$, there is no sign problem. Therefore, one can evaluate various quantities using standard Monte Carlo simulations. This opens the way to compute the canonical partition functions $Z_C(n, T, V)$ and thus the grand partition function, Z_{GC} , becomes available at both real and imaginary chemical potential due to the following fugacity expansion

$$Z_{GC}(\theta, T, V) = \sum_{n=-\infty}^{\infty} Z_C(n, T, V) \xi_B^n, \quad \xi_B = e^{N_c \mu_q / T}, \quad \theta = \frac{\mu_q}{T} = \theta_R + i\theta_I \quad (1)$$

We call this the canonical approach.

The first-order RW phase transition [3] was investigated in lattice QCD [4]. There exist lattice results and phenomenological models for the respective coefficients [5] which become Fourier coefficients for imaginary chemical potential. Computation of $Z_C(n, T, V)$ and LYZ for these models can bring more understanding and will be our next task.

Independent models for $Z_C(n, T, V)$ would be also useful for understanding the QCD phase structure at finite temperature and baryon density. In this paper we make a first step in this direction. Namely, we construct $Z_C(n, T, V)$ at high temperature above the RW transition temperature T_{RW} where lattice results for the quark number density can be well fitted by a polynomial function of the quark chemical potential. We show that our approximate solution for $Z_C(n, T, V)$ becomes exact in the infinite volume limit. Then we use these $Z_C(n, T, V)$ to compute the Lee-Yang zeros (LYZ) and show that all LYZ are on the negative real axis in the complex

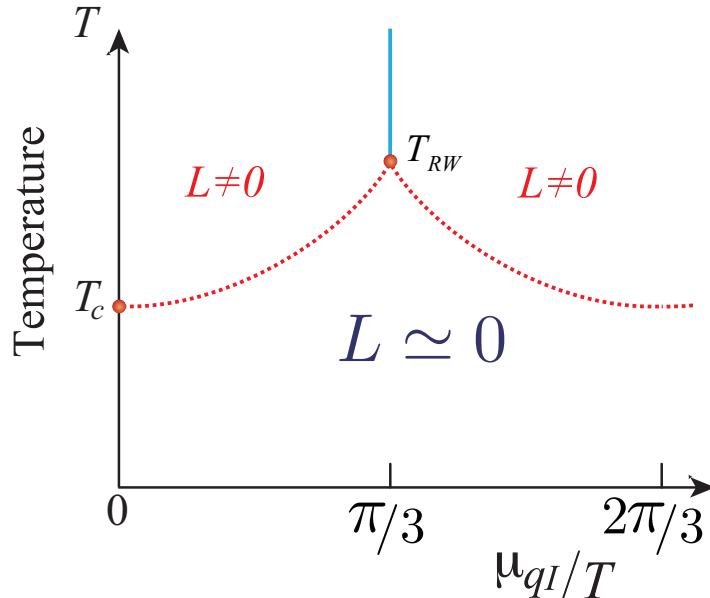


FIG. 1: Schematic figure of Roberge-Weiss phase structure at $\mu_q = \nu\mu_{qI}$. T_c is the confinement/deconfinement transition temperature at zero chemical potential, L is the Polyakov loop. The vertical line ($T \geq T_{RW}, \mu_{qI}/T = \pi/3$) shows the first order phase transition. The dashed lines show a crossover.

fugacity ξ_B plane. Nonzero linear density of LYZ at $\xi_B = -1$ corresponding to the RW transition is reached in the infinite-volume limit.

The paper is organized as follows. In Section II we describe our numerical procedure of $Z_C(n, T)$ computation as well as their asymptotic estimate based on the use of the polynomial fit to our lattice data for the quark density. In Section III we compute the LYZ and discuss the pattern of their distribution in the fugacity plane. The obtained results are summarized in the Conclusions.

Let us note that by studying QCD at imaginary chemical potential one can gain understanding not only of the RW transition but also of the critical properties of QCD related to deconfinement, chiral symmetry restoration and critical endpoint [6].

II. COMPUTATION OF THE CANONICAL PARTITION FUNCTIONS

We simulate $N_s^3 \times 4$ lattices with $N_s = 16, 20, 40$ at temperature $T/T_c = 1.35$ with $m_\pi/m_\rho = 0.8$. As in Ref. [13] we use the lattice QCD action with $N_f = 2$ clover improved Wilson quarks and Iwasaki improved

gauge field action

$$S = S_g + S_q, \quad (2)$$

$$S_g = -\beta \sum_{x,\mu\nu} (c_0 W_{\mu\nu}^{1\times 1}(x) + c_1 W_{\mu,\nu}^{1\times 2}(x)), \quad (3)$$

$$S_q = \sum_{f=u,d} \sum_{x,y} \bar{\psi}_x^f \Delta_{x,y} \psi_y^f, \quad (4)$$

where $\beta = 6/g^2$, $c_1 = -0.331$, $c_0 = 1 - 8c_1$,

$$\begin{aligned} \Delta_{x,y} = & \delta_{xy} - \kappa \sum_{i=1}^3 \{ (1 - \gamma_i) U_{x,i} \delta_{x+\hat{i},y} \\ & + (1 + \gamma_i) U_{y,i}^\dagger \delta_{x,y+\hat{i}} \} \\ & - \kappa \{ e^{a\mu_q} (1 - \gamma_4) U_{x,4} \delta_{x+\hat{4},y} \\ & + e^{-a\mu_q} (1 + \gamma_4) U_{y,4}^\dagger \delta_{x,y+\hat{4}} \} \\ & + \delta_{xy} c_{SW} \frac{\kappa}{\imath} \sum_{\mu < \nu} \sigma_{\mu\nu} P_{\mu\nu}, \end{aligned} \quad (5)$$

$P_{\mu\nu}$ is the clover definition of the lattice field strength tensor, c_{SW} is the Sheikholeslami–Wohlert coefficient. All parameters of the action, including c_{SW} value were borrowed from the WHOT-QCD collaboration paper [7].

In the following, we abbreviate the normalized canonical partition function, $Z_C(n, T, V)/Z_C(0, T, V)$, as Z_n and study the quark number density

$$\rho_q = \frac{N_q}{V} = \frac{1}{V} \frac{\partial \ln Z_{GC}(\theta, V, T)}{\partial \theta}, \quad (6)$$

where N_q is the net quark number in the lattice volume. It was observed that, at imaginary $\mu_q = \imath\mu_{qI}$, the ensemble average of the quark number density (which is also imaginary, $\rho = \imath\rho_I$) can be well approximated by an odd power polynomial at high temperatures above the RW transition temperature T_{RW} , and by the Fourier series at lower temperatures [8–13].

In Ref. [13] we developed a method to compute Z_n numerically. We fit the lattice data for the quark number density ρ_I to some function thus determining $Z_{GC}(\theta, T, V)$ up to a factor and find the Fourier transform

$$Z_C(n, T, V) = N_c \int_{-\pi/N_c}^{\pi/N_c} \frac{d\theta_I}{2\pi} e^{\imath n N_c \theta_I} Z_{GC}(\theta = \imath\theta_I, T, V) \quad (7)$$

numerically. It was found [10, 13] that at $T > T_{RW}$, i.e. above the RW transition, one can fit the lattice data for the quark number density, which is a periodic function with period $2\pi/3$, by the function

$$\hat{\rho} = a_1 \theta_I - a_3 \theta_I^3 + a_5 \theta_I^5, \quad -\pi/3 < \theta_I < \pi/3, \quad a_i > 0 \quad (8)$$

where $\hat{\rho} = \rho_q/T^3 = \hat{\rho}_R + \imath\hat{\rho}_I$. In addition to the dimensionless variable $\hat{\rho}$ characterizing the ensemble average of the quark number density we will use the variable $\varrho = \frac{n}{VT^3}$ where n is the net baryon number of a particular physical state. This variable is helpful to remember that the canonical partition functions $Z_C(n, T, V)$ are associated with a definite baryon number density ϱ .

Using formula (8) we compute Z_n at $T > T_{RW}$ for n up to some n_{max} [13] which is determined by the condition that the values of Z_n at $n > n_{max}$ computed via eq. (7) have alternating sign which is unphysical and signals that our fit-function is not suitable. That is, it cannot adequately describe high-density ($n/(VT^3) > \varrho_{max} = n_{max}/(VT^3)$) contributions to $Z_{GC}(\theta, T, V)$. It should be noticed that n_{max} depends on the volume while the corresponding (dimensionless) density ϱ_{max} is only weakly dependent on the volume and is approximately equal to 1.6 for $T/T_c = 1.35$

The reason for such unphysical behavior of Z_n (note that all Z_n are to be positive) is that eq. (8) imposes unphysical condition of a phase transition onto our finite-volume system. Indeed, the function defined by eq. (8) is discontinuous at $\theta = \pi/3 + 2\pi k/3$, $k = \pm 1, \pm 2, \dots$. Note that with $Z_n, n < n_{max}$ obtained in [13] we are able to reproduce the number density $\hat{\rho}$ dependence on θ for all θ apart from the vicinity of $\theta = \pi/3$.

Thus we have to modify the right-hand side of eq. (8) in the vicinity of the RW transition. This modification should be volume dependent and show the discontinuous behavior eq. (8) only in the infinite volume limit. To compute the quark number density ρ_{qI} in the close vicinity of the transition point $\theta = \pi/3$ is a formidable task. We follow another strategy and use an approximate analytical solution for Z_n originally suggested in [3]. In this study, we considerably improve the approximation suggested in [3] and demonstrate that this improved approximation has necessary behavior near $\theta = \pi/3$ and reproduces density (8) in the infinite volume limit.

Roberge and Weiss [3] obtained an approximate expression for Z_n in the case when $a_5 = 0$. They computed the quantities

$$Z_{nA} = \frac{\int_{-i\pi/3}^{i\pi/3} d\theta e^{-\nu F_n(\theta)}}{\int_{-i\pi/3}^{i\pi/3} d\theta e^{-\nu F_0(\theta)}} \quad (9)$$

where¹ $\nu = VT^3$ and

$$F_n(\theta) = -\varrho\theta + \frac{1}{2}a_1\theta^2 + \frac{1}{4}a_3\theta^4 \quad (10)$$

using the stationary phase method. It should be noticed that the contour of integration in (9) is the segment of imaginary axis, however, to reach the saddle point $\hat{\mu}_0$ which lies on the real axis one should deform this contour to $-i\frac{\pi}{3} \rightarrow \mu_0 - i\frac{\pi}{3} \rightarrow \mu_0 + i\frac{\pi}{3} \rightarrow i\frac{\pi}{3}$. It is reasonable to apply the method in the $V \rightarrow \infty$ limit. The stationarity condition has the form

$$\varrho - (a_1\theta + a_3\theta^3) = 0 \quad (11)$$

with the solution $\theta = \hat{\mu}_0(\varrho)$:

$$a_3\hat{\mu}_0^3 + a_1\hat{\mu}_0 - \varrho = 0. \quad (12)$$

Asymptotic expansion of the integral in the numerator of formula (9) has the form ($\nu \rightarrow \infty$)

$$Z_C(\nu\varrho, T, V) = \sqrt{\frac{2\pi}{\nu F_n''(\hat{\mu}_0)}} \exp[-\nu F_n(\hat{\mu}_0)] \left(1 + \sum_{k=1}^{\infty} \frac{\beta_k}{\nu^k}\right), \quad (13)$$

where the algorithm of determination of the coefficients β_k is described e.g. in [14].

The equation (12) can be solved by radicals:

$$\hat{\mu}_0 = \sqrt{\frac{a_1}{3a_3}} \left[(\sqrt{x^2 + 1} + x)^{1/3} - (\sqrt{x^2 + 1} - x)^{1/3} \right], \quad (14)$$

where $x = \varrho \frac{\sqrt{27a_3}}{2a_1^{3/2}}$. Then the approximate expression obtained in [3] is

$$Z_{nA} = \frac{e^{-\nu F_n(\hat{\mu}_0)}}{e^{-\nu F_0(\hat{\mu}_0)}} \quad \text{where} \quad F_n(\hat{\mu}_0) = -\frac{1}{4}(a_1\hat{\mu}_0^2 - 3\varrho\hat{\mu}_0). \quad (15)$$

This approximation consists in omitting the pre-exponential factor as well as the series in braces in formula (13)

Thus the normalized canonical partition functions Z_n can be computed both by the asymptotic formula (15) and by formula (7) numerically. The canonical partition functions Z_n determined by the former procedure are denoted Z_{nA} , by the latter — Z_{nN} . The values of Z_{nN} were computed in [13] using the quark density obtained in numerical simulations at $T/T_c = 1.35$ on lattices 4×16^3 . These values and the values of Z_{nA} computed for the respective constants a_1, a_3 are shown in Fig. 2. One can see that they agree for $n < n_{max}$. At $n > n_{max}$ Z_{nN} starts to oscillate as described above.

¹ If simulations on the $N_s^3 \times N_t$ lattice are used to determine the quark number density then $\nu = \frac{N_s^3}{N_t^3}$.

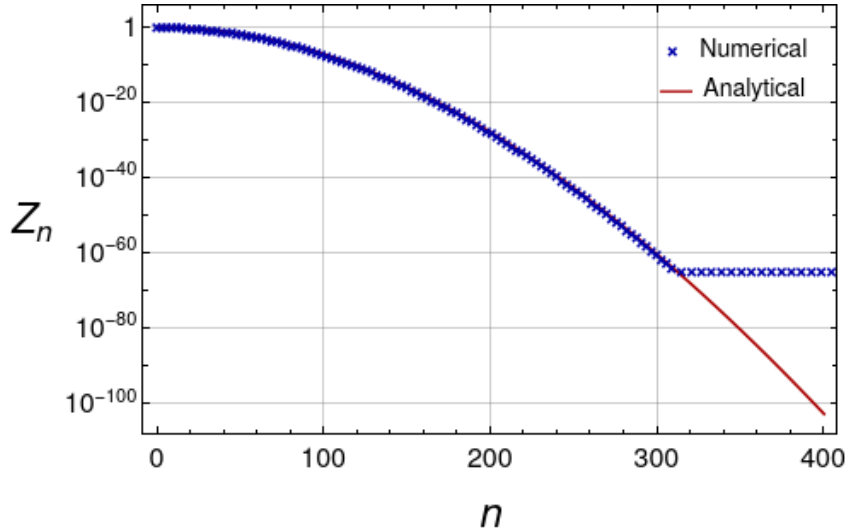


FIG. 2: Z_{nN} at $T/T_c = 1.35$ and $N_s = 16$ (blue dots) are compared with Z_{nA} (red line). For $n > 309$ only positive values of Z_{nN} are shown.

To compare Z_{nN} and Z_{nA} more explicitly we compute the relative deviation

$$R = (Z_{nN} - Z_{nA})/Z_{nN}$$

for three volumes at $\rho \leq 1.6$. We find that at $\rho < 1.5$ the relative deviation is rather small, ($R < 0.04$), but it increases rather fast reaching 0.2 at the maximal ρ for which Z_{nN} is available. We shall note that the numerical values for a_1 and a_3 were obtained on $N_s = 16$ lattices. In what follows we use same values for all volumes assuming very weak volume dependence of a_i . This is supported by our numerical results [13] on volume dependence of a_i .

In fact the expression (15) is not the full story. One can take into account the fluctuations around $\hat{\mu}_0$ to obtain

$$Z_{nA} = \frac{e^{-\nu F_n(\hat{\mu}_0)} \sqrt{F_0''(\hat{\mu}_0)}}{e^{-\nu F_0(\hat{\mu}_0)} \sqrt{F_n''(\hat{\mu}_0)}} \quad (16)$$

where

$$F_n''(\hat{\mu}_0) = (a_1 + 3a_3\hat{\mu}_0^2). \quad (17)$$

Formula (16) corresponds to the next-to-leading approximation in the asymptotic expansion (13) consisting in taking into account the pre-exponential factor. In principle, higher-order approximations can also be taken into account, however, this may be the subject of further studies. Our result eq. (16) is much closer to Z_{nN} than the result eq. (15) obtained in [3]. R goes to zero in the infinite volume limit for all values of density ρ under consideration.

Another way to check the quality of the obtained approximation for Z_n is to compute the quark number density by the formulas (eq. (5-6) in [13]):

$$\hat{\rho}_R = \frac{1}{\nu} \frac{2 \sum_{n>0} n Z_{nA} \sinh(n\theta_R)}{1 + 2 \sum_{n>0} Z_{nA} \cosh(n\theta_R)}, \quad (18)$$

$$\hat{\rho}_I = \frac{1}{\nu} \frac{2 \sum_{n>0} n Z_{nA} \sin(n\theta)}{1 + 2 \sum_{n>0} Z_{nA} \cos(n\theta_I)} \quad (19)$$

and compare it with the number density we used as the input (8). In Fig. 3 we show the quark number density $\hat{\rho}_I$ computed via Z_{nA} in the vicinity of the critical value $\theta = \pi/3$. The volume dependence of the density becomes visible: with increasing volume the number density approaches a step function, i.e. the first order phase transition appears in the infinite volume limit.

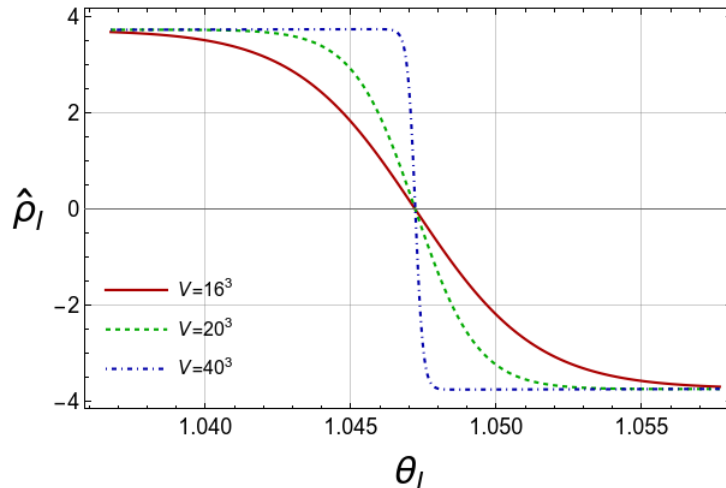


FIG. 3: The quark number density computed using Z_{nA} at $T/T_c = 1.35$ for imaginary chemical potential for three volumes and $\varrho = 5\varrho_{max}$ over a restricted range near $\pi/3$.

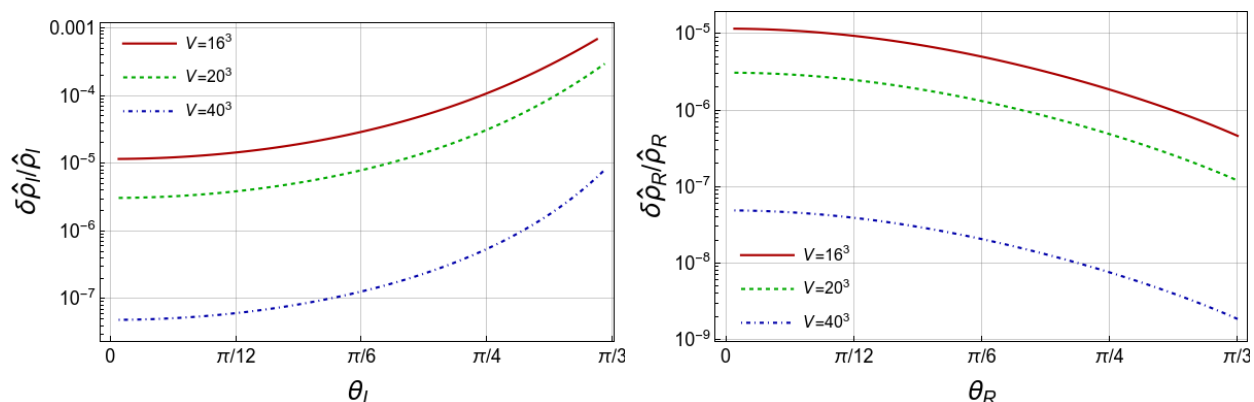


FIG. 4: Relative deviation of the quark number density computed using Z_{nA} at $T/T_c = 1.35$ for imaginary chemical potential (left panel) and the real chemical potential (right panel).

The relative deviation for the quark number density is shown in Fig. 4 for three spatial volumes. In the left panel it is shown for imaginary μ_q . The deviation is small and shows very fast decreasing with increasing V . Note that the relative deviation increases near $\theta_I = \pi/3$ since eq. (8) gives a correct number density in this range in the infinite volume limit only. In the right panel we show the relative deviation for real chemical potentials. Again we see that this relative deviation is small and decreases with an increase of the volume.

For $a_5 \neq 0$, an explicit solution of eq. (8) is not available. However, considering a_5 as a small parameter we find an approximate solution, details of computation are presented in Appendix.

Since $a_5 = 0$ within error bars at $T = 1.35T_c$, we estimated the corrections due to higher-order terms in the case $T = 1.2T_c$. We find a good qualitative agreement between Z_{nN} and Z_{nA} at $n < 291$ where Z_{nN} are available: $|R| < 0.04$ at $n < 200$ and runs up to 0.4 as n increases until 290.

III. EVALUATION OF LEE-YANG ZEROS

Lee-Yang zeros are zeros of the grand partition function $Z_{GC}(\theta, T, V)$, considered as a polynomial of the baryon fugacity $\xi_B = e^{\mu_B/T} = e^{N_c\theta}$, where $\mu_B = 3\mu_q$ is baryon chemical potential. In the finite volume V , $Z_{GC}(\theta, T, V)$ has the form

$$Z_{GC}(\theta, T, V) = \sum_{n=-n_{max}}^{n_{max}} Z_C(n, T, V) \xi_B^n = e^{-n_{max}N_c\theta} \sum_{n=0}^{2n_{max}} Z_C(n - n_{max}, T, V) \xi_B^n, \quad (20)$$

where $n_{max} = 2N_c N_f N_s^3 L_t$ for Wilson fermions. Computation of zeros of the high degree polynomial, eq.(20), is in general very difficult task. In this work we employ a very efficient package, MPSolve v.3.1.8 (Multiprecision Polynomial Solver) [15, 16], which provides calculation of polynomial roots with arbitrary precision.

In eq.(20) we rewrite $Z_{GC}(\theta, T, V)$ as a polynomial of degree $2n_{max}$ whose roots represent the values of the Lee-Yang zeros (LYZ) in the complex ξ_B -plane. Coefficients $Z_C(n, T, V) \equiv Z_{nA}$ are computed using eq.(16) with the GNU MPFR Library for multiple-precision floating-point computations. We performed calculations using the MPFR library with an accuracy from 1000 to 4000 digits. We found that 1000 digits is enough for MPSolve package to calculate LYZ for polynomial with degree less than 20000. We also checked that to calculate LYZ for polynomials of degree greater than 30,000, it is necessary to use Z_{nA} calculated with an accuracy of more than 4000 digits.

In practical lattice calculations at fixed lattice spacing a both $V/a^3 = N_s^3$ and the limits in the sum eq.(20) (which we denote as N_{max} in what follows) are finite. Thus we have to study dependence of the Lee-Yang zeros on N_{max} and N_s to make a conclusion about the infinite-volume limit. Analytical expression for the coefficients of the polynomial together with the use of MPSolve package allows us to work with an arbitrary degree of the polynomial limited only by the computational cost of LYZ calculation and to substantially improve our previous results [17] for $T > T_{RW}$. Our main goal is to understand the properties of LYZ in the vicinity of the RW phase transition at $\xi_B = -1$.

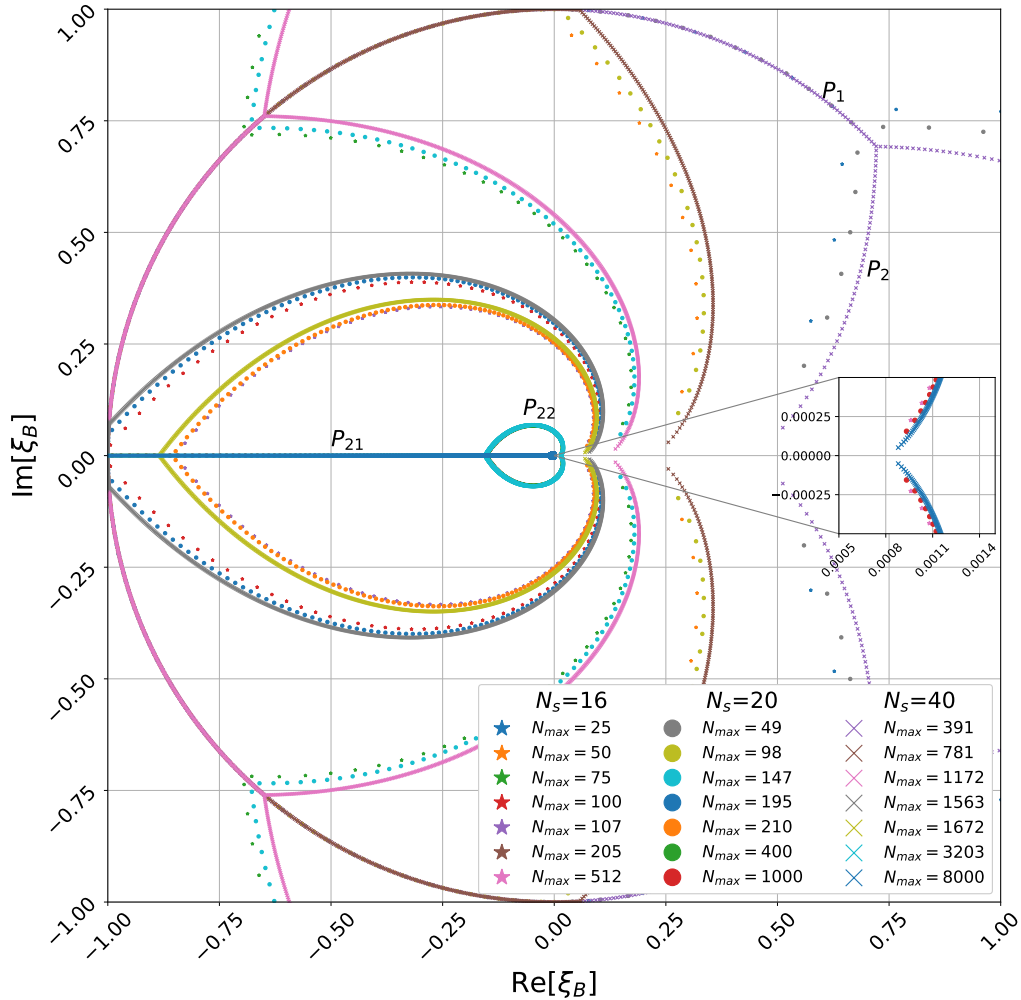


FIG. 5: LYZ distribution for $T/T_c = 1.35$

In Fig.5 the results for LYZ are presented for three volumes with $N_s = 16, 20, 40$ and six values of N_{max} for each volume. These values of N_{max} change with volume and correspond to six volume independent values of the maximal quark number density $\rho_{max} = N_{max}/(VT^3)$. At $VT^3 = \frac{N_s^3}{N_t^3} = 64$ we start with $\rho_{max} = 25/64 = 0.39$,

and increase it up to $\varrho_{max} = 512/64 = 8.0$.

In [17] it was found that the dependence on ϱ_{max} is much more pronounced than the dependence on the volume. It was shown in [17] that for small ϱ_{max} LYZ consist of two parts: the former part, P_1 , comprises the LYZ distributed along the unit circle $|\xi_B| = 1$ and the latter, P_2 , represents a curve starting on the circle at the end point of P_1 and extending towards the real positive axis. With increasing volume the endpoint of P_2 tends to approach the real axes.

It was demonstrated in [17] that P_1 shrinks to $\xi_B = -1$ with increasing ϱ_{max} . Respectively, one end of P_2 moves along the unit circle towards $\xi_B = -1$ while the other end slowly moves in the direction of $\xi_B = 0$. We now confirm these observations as can be seen from comparison of LYZ for $\varrho_{max} = 0.39, 0.78, 1.17, 1.56, 1.67, 3.20, 8.00$ in Fig.5. But due to computations with much higher maximal density $\varrho_{max} = 3.2, 8.0$ we discover the correct properties of the LYZ in the limit $N_{max} \rightarrow n_{max}$.

In Fig.5 one can see that P_1 disappears completely at $\varrho_{max} > \varrho_c \approx 1.6$. It is worth noting that this is approximately the same value of the quark density which is reachable in computations of Z_{nN} . It is natural to assume that the leading contributions to the grand canonical partition function come from all densities over the range $\varrho < \varrho_c$ and thus neglecting even part of them gives rise to unphysical results for Lee-Yang zeros (the P_1 part on the unit circle).

It should be noticed that the first real negative LYZ appears also when ϱ_{max} becomes as much as ϱ_c for all volumes under consideration.

The P_2 line splits into two parts for $\varrho_{max} > 1.6$: P_{21} consisting of LYZ on the negative real axis $-1 < \xi_B < -\xi_{B0}$, $\xi_{B0} > 0$, with ξ_{B0} moving toward zero with increasing $\hat{\rho}_{max}$ and a curly part P_{22} connecting $-\xi_{B0}$ with the point slightly above the positive real axis. As we mentioned above, this point moves to the real axis in the infinite volume limit for fixed ϱ_{max} . When we first increase ϱ_{max} to its maximal value for a given volume (in practical terms this implies the extrapolation to the infinite value) and then take the infinite volume limit, we find that the right end of P_{22} goes to $\xi_B = 0$. We also find an indication that in the limit of infinite ϱ_{max} $\xi_{B0} = 0$. We thus conclude that in the infinite volume limit all LYZ lie on the real negative axis.

Thus we see very strong dependence of LYZ on ϱ_{max} . It can be seen in Fig.5 that the finite volume effects are rather mild. For the maximal value of ϱ_{max} shown in the figure one can see these effects in the enlarged insertion only.

Next we describe the properties of the LYZ on the real-negative axis. We found that for a fixed volume they start to appear when N_{max} exceeds some value roughly equal to $\varrho_c \cdot VT^3$. The LYZ most close to $\xi = -1$ appear first and, with increasing N_{max} , more and more remoted from -1 LYZ also appear. This property of LYZ is seen in Fig.5.

The distance between adjacent LYZ on the real negative semiaxis is shown on the left panel of Fig.6 as a function of θ_R at $\theta_I = \frac{\pi}{3}$ for $N_s = 16, 20, 40$. The density of LYZ, which is proportional to the inverse of this quantity, is actually independent of the volume at $|\theta_R| > 0.5$ and shows only a weak dependence on the volume in the neighborhood of $\theta = \frac{i\pi}{3}$. Thus we conclude that in the infinite-volume limit the density of LYZ does not vanish over the entire negative real semiaxis in the fugacity plain including the point $\xi_B = -1$, where the RW phase transition takes place. Yet another evidence for our conclusion comes from the dependence of the $|\xi_{cl} + 1|$ on the volume, where ξ_{cl} is the LYZ closest to -1 . This dependence is shown on the right panel of Fig.6, where the constant A is an estimate of the LYZ density at $\xi_B = -1$, which ceases to depend on the volume for the lattice sizes under consideration.

Thus the linear density of LYZ remains finite in the infinite-volume limit. According to the criterion suggested in [18], the phase transition occurs at $Im(\mu) = \pi$.

IV. CONCLUSIONS

We have studied $N_f = 2$ lattice QCD in the deconfinement phase above T_{RW} at $T/T_c = 1.35$. Our goal was to compute the distribution pattern of LYZ in the complex fugacity ξ_B plain and to demonstrate the existence of the LYZ close to $\xi = -1$ corresponding to the first-order RW transition at imaginary quark chemical potential.

In our earlier work [17] we had performed computations of LYZ at $T > T_{RW}$ using a limited number of Z_{nN} - canonical partition functions computed numerically via the Fourier transform. In this work, to overcome this restriction, we have used the approximate analytical expression Z_{nA} . We demonstrated that Z_{nA} agree very well with values of Z_{nN} where the latter are available and reproduce the input expression for the quark number density. In both cases the agreement improves with increasing volume. Using Z_{nA} we have obtained the behavior for the quark number density in the vicinity of the RW phase transition at $\theta_I = \pi/3$ which is consistent with first principles.

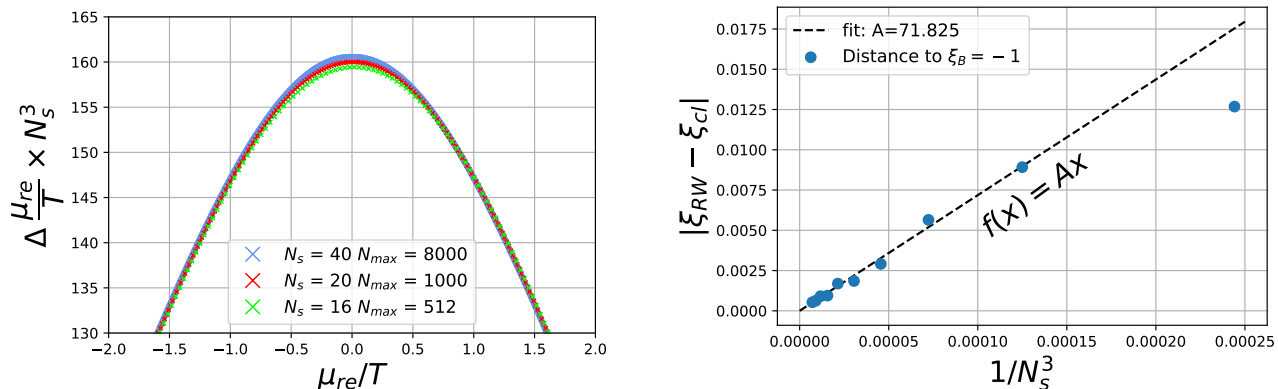


FIG. 6: Left: the dependence of the distance between adjacent LYZ on the real part of the quark chemical potential at $\theta_I = \pi/3$ for different lattice sizes. Right: The volume dependence of the distance between the point $\xi_B = -1$ and the nearest LYZ.

We have demonstrated that, in the infinite volume limit, there appears a discontinuity in the dependence of $\hat{\rho}$ on θ_I indicating the first-order transition behavior.

After we made sure that Z_{nA} works very well we computed the LYZ. Apart from increasing the available maximal density ϱ_{max} which is now restricted only by the computation resources, we also used more effective procedure to compute LYZ. We have used the effective MPSolve library with arbitrary precision. Our multi-precision computations have been performed with 4000 significant digits.

We confirmed our previous results obtained in [17] with restricted ϱ_{max} about strong dependence of LYZ on ϱ_{max} and comparatively weak volume dependence.

Then, increasing ϱ_{max} , we have discovered that the the LYZ appear on the ξ negative real half-axis and in the infinite volume limit they fill in the full $Re(\xi) \leq 0$ range. This is in agreement with findings of [6]. We demonstrated that in the limit of high ϱ_{max} there are no LYZ away from the ξ negative real axis. We have found that nonvanishing density of LYZ at $\xi = -1$ corresponding to the RW first order phase transition at $T > T_{RW}$ and imaginary quark chemical potential appear only in the infinite volume limit.

Our result demonstrates necessity of using sufficiently high values of ϱ_{max} to obtain correct results for LYZ. We believe that our results obtained at high temperature where phase transitions are absent at real chemical potential will be useful for computation of LYZ at low temperature where phase transition or cross-over is present. This work is now underway.

Acknowledgments

This work was supported by the Russian Foundation for Basic Research via grant 18-02-40130 mega and partially carried out within the state assignment of the Ministry of Science and Higher Education of Russia (Project No. 0657-2020-0015). Computer simulations were performed on the FEFU GPU cluster Vostok-1, the Central Linux Cluster of the NRC "Kurchatov Institute" - IHEP, the Linux Cluster of the NRC "Kurchatov Institute" - ITEP (Moscow). In addition, we used computer resources of the federal collective usage center Complex for Simulation and Data Processing for Mega-science Facilities at NRC Kurchatov Institute, <http://ckp.nrcki.ru/>. Participation of Denis Boyda at the earlier stages of this work is gratefully acknowledged.

-
- [1] S. Borsanyi, Z. Fodor, J. N. Guenther, R. Kara, P. Parotto, A. Pasztor, C. Ratti and K. K. Szabo, [arXiv:2202.05574 [hep-lat]].
 - [2] D. Bollweg, J. Goswami, O. Kaczmarek, F. Karsch, S. Mukherjee, P. Petreczky, C. Schmidt and P. Scior, [arXiv:2202.09184 [hep-lat]].
 - [3] A. Roberge and N. Weiss, Nucl. Phys. B275, 734, 1986.
 - [4] C. Bonati, G. Cossu, M. D'Elia and F. Sanfilippo, Phys. Rev. D **83** (2011), 054505 [arXiv:1011.4515 [hep-lat]].

- [5] V. Vovchenko, J. Steinheimer, O. Philipsen and H. Stoecker, Phys. Rev. D **97** (2018) no.11, 114030, [arXiv:1711.01261 [hep-ph]].
- [6] G. A. Almasi, B. Friman, K. Morita, P. M. Lo and K. Redlich, Phys. Rev. D **100**, no.1, 016016 (2019) [arXiv:1805.04441 [hep-ph]].
- [7] S. Ejiri *et al.* [WHOT-QCD], Phys. Rev. D **82** (2010), 014508 [arXiv:0909.2121 [hep-lat]].
- [8] T. Takaishi, P. de Forcrand, A. Nakamura, PoS LAT 2009 (2009) 198, arXiv:1002.0890 [hep-lat].
- [9] M. D’Elia, F. Sanfilippo, Phys. Rev. **D80** (2009) 014502, arXiv:0904.1400 [hep-lat].
- [10] J. Takahashi, H. Kouno, M. Yahiro, Phys. Rev. **D91** (2015) 014501, arXiv:1410.7518 [hep-lat].
- [11] M. D’Elia, G. Gagliardi, F. Sanfilippo, Phys. Rev. **D95** (2017) 094503, arXiv:1611.08285 [hep-lat].
- [12] J. Gunther, R. Bellwied, S. Borsanyi, Z. Fodor, S.D. Katz, A. Pasztor, C. Ratti, EPJ Web Conf. 137 (2017) 07008, arXiv:1607.02493 [hep-lat].
- [13] V.G.Bornyakov, D.L.Boyda, V.A.Goy, A.V.Molochkov, Atsushi Nakamura, A.A.Nikolaev, V.I. Zakharov Phys. Rev. **D95**, (2017) 094506.
- [14] Lavrentev M.A., Shabat B.V. “Methods of the theory of function of complex variable”, Nauka: Moscow, 1987.
- [15] Bini, Dario A., Fiorentino, Giuseppe, Numerical Algorithms 23.2-3 (2000): 127-173.
- [16] Bini, Dario A., and Robol, Leonardo. Journal of Computational and Applied Mathematics 272 (2014): 276-292.
- [17] M. Wakayama, V. Bornyakov, D. Boyda, V. Goy, H. Iida, A. Molochkov, A. Nakamura and V. Zakharov, Phys. Lett. B **793**, 227-233 (2019) doi:10.1016/j.physletb.2019.04.040 [arXiv:1802.02014 [hep-lat]].
- [18] , T. D. Lee and Chen-Ning Yang, Phys. Rev. **87** (1952) pp. 410–419.

Appendix A: Corrections for $a_5 \neq 0$.

The approximate solution $\hat{\mu}_0$ of the equation

$$a_5 \hat{\mu}_0^5 + a_3 \hat{\mu}_0^3 + a_1 \hat{\mu}_0 - \varrho = 0 \quad (\text{A1})$$

up to the order a_5^2 has the form

$$\hat{\mu} = \hat{\mu}_0 + a_5 \hat{\mu}_1 + a_5^2 \hat{\mu}_2, \quad (\text{A2})$$

where

$$\hat{\mu}_1 = -\frac{\hat{\mu}_0^5}{a_1 + 3a_3 \hat{\mu}_0^2}, \quad (\text{A3})$$

$$\hat{\mu}_2 = -\frac{5\hat{\mu}_1 \hat{\mu}_0^4 + 3a_3 \hat{\mu}_1^2 \hat{\mu}_0}{a_1 + 3a_3 \hat{\mu}_0^2}. \quad (\text{A4})$$

Then we follow the procedure described in eqs. (9-16) and obtain

$$Z_{nA} = \frac{e^{-\nu F_n(\hat{\mu})} \sqrt{F_0''(\hat{\mu})}}{e^{-\nu F_0(\hat{\mu})} \sqrt{F_n''(\hat{\mu})}}, \quad (\text{A5})$$

where

$$F_n(\hat{\mu}) = -\frac{1}{4}(a_1 \hat{\mu}_0^2 - 3\hat{\rho} \hat{\mu}_0 + a_5 f_1(\hat{\mu}_0) + a_5^2 f_2(\hat{\mu}_0) + O(a_5^3)), \quad (\text{A6})$$

$$F_n''(\hat{\mu}) = (a_1 + 3a_3 \hat{\mu}_0^2 + a_5 f_3(\hat{\mu}_0) + a_5^2 f_4(\hat{\mu}_0) + O(a_5^3)) \quad (\text{A7})$$

and

$$f_1(\hat{\mu}_0) = \frac{2}{3} \hat{\mu}_0^6, \quad (\text{A8a})$$

$$f_2(\hat{\mu}_0) = -\frac{2\hat{\mu}_0^{10}}{a_1 + 3a_3 \hat{\mu}_0^2}, \quad (\text{A8b})$$

$$f_3(\hat{\mu}_0) = \hat{\mu}_0^4 \left(3 + \frac{2a_1}{a_1 + 3a_3 \hat{\mu}_0^2} \right), \quad (\text{A8c})$$

$$f_4(\hat{\mu}_0) = -\hat{\mu}_0^8 \frac{20a_1^2 + 87a_1 a_3 \hat{\mu}_0^2 + 99a_3^2 \hat{\mu}_0^4}{(a_1 + 3a_3 \hat{\mu}_0^2)^3}. \quad (\text{A8d})$$

To compute Z_{nA} for $T/T_c = 1.20$ we use $a_1 = 4.409, a_3 = 1.032, a_5 = -0.165$ [13] in eq. (8). It should be noted that with this set of constants a_i is not applicable at large real chemical potential since the quark density becomes negative. To keep the density positive we should assume that the coefficient a_7 which was not determined in [13] is positive.